

Long-Lived Correlated Triplet Pairs in a π -Stacked Crystalline Pentacene Derivative

Brendan D. Folie,[†] Jonah B. Haber,[†] Sivan Refaely-Abramson,^{†,§} Jeffrey B. Neaton,^{†,§,#} and Naomi S. Ginsberg^{*,†,‡,||,⊥,#}

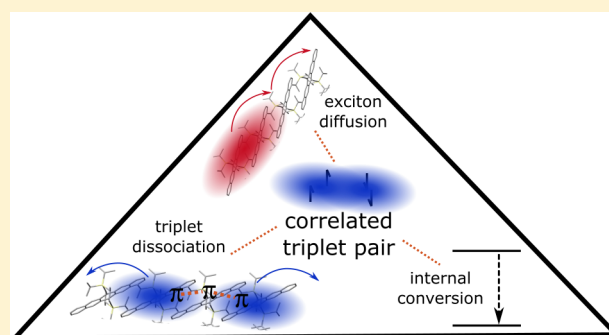
[†]Department of Physics and [‡]Department of Chemistry, University of California, Berkeley, California 94720, United States

[§]Molecular Foundry, ^{||}Molecular Biophysics and Integrated Bioimaging, and [⊥]Materials Sciences Divisions, Lawrence Berkeley National Laboratory, Berkeley, California 94720, United States

[#]Kavli Energy NanoSciences Institute, Berkeley, California 94720, United States

Supporting Information

ABSTRACT: Singlet fission is the spin-conserving process by which a singlet exciton splits into two triplet excitons. Singlet fission occurs via a correlated triplet pair intermediate, but direct evidence of this state has been scant, and in films of TIPS-pentacene, a small molecule organic semiconductor, even the rate of fission has been unclear. We use polarization-resolved transient absorption microscopy on individual crystalline domains of TIPS-pentacene to establish the fission rate and demonstrate that the initially created triplets remain bound for a surprisingly long time, hundreds of picoseconds, before separating. Furthermore, using a broadband probe, we show that it is possible to determine absorbance spectra of individual excited species in a crystalline solid. We find that triplet interactions perturb the absorbance, and provide evidence that triplet interaction and binding could be caused by the π -stacked geometry. Elucidating the relationship between the lattice structure and the electronic structure and dynamics has important implications for the creation of photovoltaic devices that aim to boost efficiency via singlet fission.



INTRODUCTION

Singlet fission converts a singlet exciton into two triplet excitons via a multistep process. The initially generated triplets are entangled into an overall spin-0 state, known as the correlated triplet pair,^{1–3} and denoted (TT)¹. The correlated triplet pair eventually dissociates into a pair of noninteracting triplets, although long-range spin correlations may persist.^{1,3} The correlated triplet pair is thus the linchpin of singlet fission: its electronic structure affects the dynamics of triplet formation and triplet separation, both of which are crucial for triplet harvesting. A proper understanding of the correlated triplet pair could therefore improve singlet fission-based photovoltaic devices, since although efficiencies of up to 45% are possible in theory,² and progress has been made,^{4,5} overall efficiencies remain low. Little is known about the energetics or kinetics of the correlated triplet pair, in part because it is often short-lived, and may be nearly indistinguishable spectroscopically from dissociated triplets. Direct measurements of the correlated triplet pair will both improve our fundamental understanding of singlet fission and lead to better design principles for devices.

The basic mechanism of fission remains a heated topic of research.^{6–12} The fission rate is thought to depend strongly on the nature of the excited singlet and triplet states and on the associated details of the electronic structure—in particular on the presence of charge transfer (CT) states^{13–15}—through

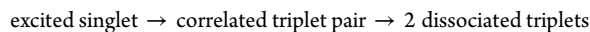
orbital overlap^{6,7} and vibronic coupling.^{7,16,17} As a result, fission is sensitive to crystal structure: two polymorphs of the same material can have fission rates that vary by an order of magnitude or more,^{18–22} and within a disordered film fission can preferentially occur at specific sites.²³ Such sensitivity makes it difficult to predict a priori whether or how rapidly fission will occur in a given material, but one design principle that people have used to guide the quest for high efficiency fission devices is to engineer π -stacking. π -Stacking occurs when aromatic rings pack face to face, creating overlap between the π -orbitals on neighboring molecules.²⁴ π -Stacking often leads to high carrier mobilities, strong coupling between electrons on neighboring molecules, and relatively delocalized excitons.^{25–27} Due to this strong coupling, it is generally assumed that slip-stacked crystals with strong π - π interactions can potentially yield high fission efficiencies and rates.^{2,15,28} Two recent theoretical studies have, however, found that strong coupling between singlets²⁹ or between triplets⁸ may have a detrimental effect on the fission rate. In addition, derivatives of the small-molecule semiconductor thiophene-capped diketopyrrolopyrrole (TDPP) display strong π -stacking, yet analysis of transient absorption data indicates that an intermediate state

Received: November 30, 2017

hypothesized to be $(TT)^1$ forms on a time scale between 1 and 16 ps and that the triplet pairs dissociate on a time scale between 20 and 1600 ps.³⁰ These time scales are slow compared to those for pentacene films (~ 100 fs),³¹ even though pentacene's herringbone structure leads to weaker electronic coupling.⁷ Could strong orbital interaction hinder singlet fission? Is the correlation between strong coupling and slower triplet generation/separation a general effect, or is it specific to TDPP? One prototypical π -stacked system that could help shed light on these questions is crystalline 6,13-bis(triisopropylsilyl)ethynyl)pentacene, or TIPS-pentacene (TIPS-Pn). Although TIPS-Pn is known to undergo fission,^{32,33} the time scale has been unclear: for amorphous films, it has been reported to occur on both a 100 fs time scale³⁴ and a 1 ps time scale.³⁵ Turning to nanoparticles, heterogeneity within a nanoparticle and diffusion between different regions of it have been implicated as leading to multiple fission time scales: 220 fs and 1.37 ps in one work,³⁶ and 2.9 and 169 ps in another.³⁷ More recent work asserts that the time scale is 100 fs in crystalline and 1.2 ps in amorphous nanoparticles.³⁸ Interestingly, it has been asserted that increasing crystallinity leads to both more³⁸ and less³⁷ efficient fission, a discrepancy that has been attributed to different sample preparation protocols. A perfectly crystalline film has produced a fairly slow fission time scale of 5 ps.³⁹ Further study is needed to understand the fission time scale, and how it is controlled by crystallinity, which for TIPS-Pn goes hand in hand with π -stacking.

Experimental knowledge of the correlated triplet pair is limited. In pentacene and hexacene, photoemission spectroscopy has been used to track the dynamics of the triplet pair and show that it can form concurrently with the singlet.^{40,41} Some of the most insightful experiments have been performed on tetracene and TIPS-tetracene, because they exhibit slow fission and long triplet lifetimes. These longer lifetimes make it possible to track oscillations between magnetic sublevels using delayed fluorescence^{42,43} or to measure triplet triplet interactions and coherence using electron spin resonance.⁴⁴ These experiments reveal that triplet pairs can remain proximal and coherent for a long time (10s to 100s of ns), and reveal two types of triplet-triplet interaction: a weak magnetic dipolar regime,⁴² and a strong exchange-coupled regime.⁴⁴ Similarly, spin correlations and triplet dissociation have been observed in isolated pentacene dimers,⁴⁵ although the electronic structure and dynamics of such dimers can differ from those in films, where wave functions can extend beyond a dimer of molecules.

Ultrafast optical observations of the triplet pair have been limited to using global analysis on bulk transient absorption (TA) data to argue for the existence of an intermediate state between the initially generated singlets and long-lived triplets. Such experiments reveal the transient absorption spectrum of the triplet pair, and provide some insight into the kinetics, although the models used thus far have been simplified to



This experimental process has been carried out for crystalline tetracene,⁴⁶ TIPS-tetracene in solution⁴⁷ and crystalline form,⁴⁸ colloidal aggregates of pentacene derivatives,⁴⁹ and polycrystalline films of TDPP derivatives.³⁰ A recently published work studied amorphous films of several organic semiconductors, and, using global analysis of temperature dependent TA data, found evidence of a bound correlated triplet pair.⁵⁰ Overall, our understanding of the interactions between correlated triplets

remains limited, particularly in systems in which the triplets form on ultrafast time scales.

We study the correlated triplet pair using polarization sensitive transient absorption microscopy (TAM) with a white light probe. Like ordinary TA, TAM uses ultrafast laser pulses to track excited state dynamics. Focusing the laser pulses through a microscope objective allows for the study of individual nanoscale objects^{51,52} or for better resolution of submicron processes in macroscopic materials.^{53,54} One can also study individual domains of polycrystalline samples. TAM can reveal interdomain heterogeneity⁵⁵ and permits selective coupling to different transition dipole moments (TDMs) via rotation of the probe polarization. Figure 1a,b show top and

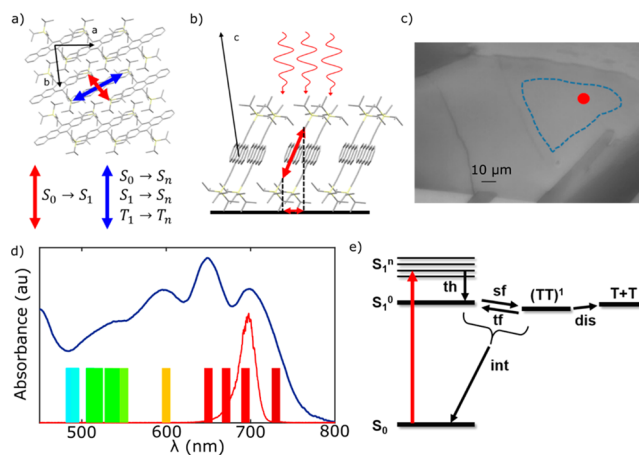


Figure 1. Crystal structure and optical properties of TIPS-pentacene (TIPS-Pn). (a) Top-down and (b) side-on view of a single layer shows that the molecules pack in a brickwork configuration, leading to strong π -stacking. Two transition dipole moments (TDMs) are shown, red along the short axis and blue along the long axis of the pentacene core. (c) Optical image of a representative TIPS-Pn domain. The red dot is $7.5 \mu\text{m}$ across, the $1/e^2$ size of a typical pump. All data were taken within the homogeneous area bounded by the blue dashed line. (d) Absorption spectrum of TIPS-Pn. The pump laser spectrum, centered at 700 nm, is seen to primarily excite the $S_0 \rightarrow S_1$ transition. Vertical bars represent the 12 different probes derived from a white light spectrum. (e) A Jablonski diagram of states and processes considered in this work. States are the ground state, S_0 , first excited state, S_1^0 , first excited state with vibrational energy, S_1^n , correlated triplet pair, $(TT)^1$, and two dissociated triplets, $T + T$. Processes are thermalization (th), internal conversion (int), singlet fission (sf), triplet fusion (tf), and triplet dissociation (dis). The pump excites from S_0 to S_1^n (red vertical arrow). Internal conversion occurs from both S_1 and $(TT)^1$.

side views of a crystal of TIPS-Pn; π -stacking is evident. The $S_0 \rightarrow S_1$ TDM is known to lie along the short axis of the pentacene core⁵⁶ (red arrow). We find that other TDMs, such as that for $S_1 \rightarrow S_m$, lie along the long axis of pentacene (blue), nearly perpendicular to the $S_0 \rightarrow S_1$ TDM. These TDMs produce TA signals of opposite sign: the first creates ground state bleach (GSB), whereas the second creates excited state absorption (ESA). Traditional TA on amorphous or polycrystalline films averages over many randomly oriented domains, causing these competing signals to obscure each other. TAM, however, focuses on a single domain, and by varying the probe polarization we individually track the signal due to each TDM, leading to a more complete understanding of the excited state dynamics.^{41,57}

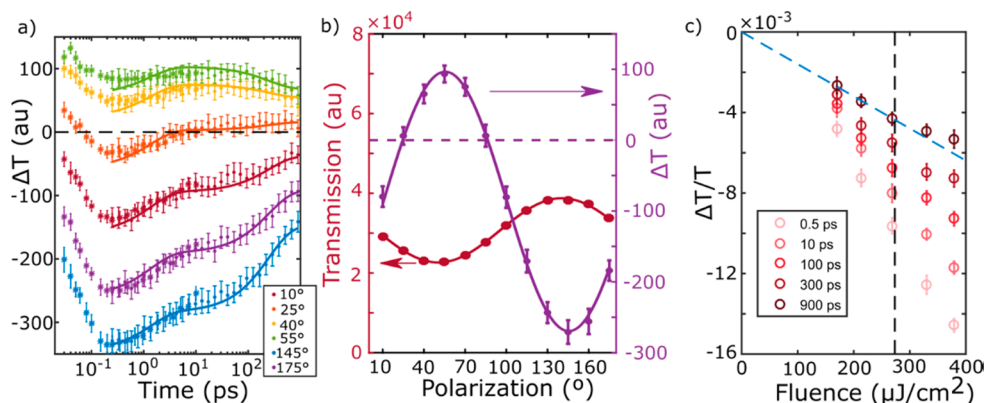


Figure 2. Degenerate (700 nm pump and probe) Transient absorption (TA) on TIPS-Pn. A full TA data set, $\Delta T(\theta, \tau)$, is visualized via selected slices (a) at constant θ and (b) at constant $\tau = 10$ ps. Two data sets are shown in (a), one focusing on short τ (30 fs–10 ps) and one on longer τ (250 fs–900 ps). Solid lines are a fit to a kinetic model. ΔT at 10 ps in (b) (purple, right axis) is shown juxtaposed with linear transmission (red, left axis) to facilitate analysis. Both curves are fit to eq 1. Although the respective local maxima and minima of these curves occur at $\sim 55^\circ$ in the lab frame, this value does not have any connection with the canonical “magic angle”, whose utility is lost when working with an individual anisotropic crystalline domain. (c) Peak fluence dependence measurements at several different τ . At early times the signal is linear, but at $\tau = 900$ ps the signal deviates from linearity (diagonal dashed line) around $300 \mu\text{J}/\text{cm}^2$, indicating annihilation via diffusion. Vertical line indicates the fluence used in our experiments, to ensure we are in a linear regime.

Here we perform white light TAM on individual crystalline domains of solution-cast TIPS-Pn to extract the spectroscopic signature of the correlated triplet pair. We establish a kinetic model and report values for all of its relevant rate constants. We determine the binding energy between correlated triplets, and find that it significantly hinders triplet separation. We report the absorbance spectrum of each excited state in the kinetic model, and reveal that the triplet–triplet interaction systematically perturbs the absorbance. We discuss these findings in terms of π -stacking and its effect on electronic structure. Finally, we consider implications for devices, and speculate that slow triplet dissociation may, counterintuitively, make singlet-mediated diffusion^{39,58} more efficacious, ultimately allowing for thicker active layers of TIPS-Pn.

EXPERIMENTAL SECTION

TIPS-Pn was purchased as powder from Sigma-Aldrich, dissolved in toluene to a concentration of 5 mg/mL, and passed through a $0.45 \mu\text{m}$ filter. Approximately $140 \mu\text{L}$ of this solution was deposited onto a glass coverslip that had been sonicated in both acetone and isopropyl alcohol and then treated with trichloro(phenethyl)silane. The substrate was heated to 55°C and covered as the sample dried. Crystalline domains were located by inspection. An example is shown in Figure 1c.

An 80 MHz mode-locked Ti:sapphire Coherent Vitera oscillator was used to create a seed pulse, which fed a Coherent Legend-Elite regenerative amplifier. The output at a wavelength of 800 nm and repetition rate of 5 kHz was split, and one line was used to pump an optical parametric amplifier (Coherent OPerA Solo) and create the 700 nm pump pulse. This pulse was split to create a degenerate probe pulse. The 800 nm output was also focused onto a sapphire plate to create white light, which was filtered through a 10 nm bandpass filter before impinging on the sample to select a desired nondegenerate probe wavelength. Spectral filtering limits the temporal resolution but was necessary to prevent sample damage. Figure 1d shows the pump pulse spectrum (red) overlaid on the linear absorption spectrum of TIPS-Pn (blue). Each vertical bar represents the wavelength range of a probe employed in this work.

The pump and probe were spatially overlapped within a single crystalline domain of TIPS-Pn. As shown in Figure 1c, the beams fit easily within single domains, which can be up to $100 \mu\text{m}$ in size. We measured the transient absorption signal as a function of pump–probe delay time and probe polarization for multiple probe wavelengths.

Data on multiple individual domains were obtained and compared. For more details on the experimental setup see Figures S1–S2, associated text, and our previous work.⁵⁹

RESULTS

We first describe TAM measurements performed using a degenerate copy of the pump as the probe beam. Analysis of these data lead us to develop a kinetic model for the exciton dynamics in TIPS-pentacene domains. We then turn to TAM performed with a white light pulse, which is filtered to produce a broad spectrum of probes. The kinetic model obtained from the degenerate experiment is fit to the white light data in order to both substantiate the model and extract additional information about interactions between the correlated triplets.

Degenerate TAM data are shown in Figure 2a,b. The transient absorption signal, ΔT , is a function of both pump–probe delay time, τ , and probe pulse polarization, θ . Each of the curves shown in Figure 2a represents the system’s time evolution at a different, specific, fixed θ . We find three clear time scales for all curves: the signal drops over ~ 100 fs, rises over ~ 1 ps, and tends toward zero over several hundred ps, consistent with previous measurements.³⁵ The polarization resolution of TAM permits us to observe both GSB and ESA, as evidenced by the fact that we see curves with both positive and negative values of ΔT . To more clearly see the balance between GSB and ESA, we fix τ at 10 ps and plot ΔT as a function of θ (Figure 2b, purple). The curve is fit to

$$\Delta T(\theta) = A \cos^2(\theta - \theta_0) + C \quad (1)$$

The linear transmission is also shown as a function of polarization (red), and its minimum indicates the orientation of the GSB TDM, which is along the short axis of the pentacene core.⁵⁶ Because $\Delta T < 0$ when the transmission is high (absorption is low), we deduce that the GSB and ESA TDMs are not parallel. Both ΔT and T are reported in the same units, allowing one to see that the fractional change in optical density is small—in this case on the order of 0.01.

For our subsequent analysis, it is crucial that all data are collected in a regime free of higher order nonlinear processes. To ensure that this is the case, we measure $\Delta T/T$ as a function

of pump fluence for several delay times, and plot the results in Figure 2c and Figure S3. At higher fluence (higher exciton density), the signal saturates, particularly for $\tau \geq 300$ ps. This saturation indicates that excitons created in different parts of the sample are interacting due to diffusion. We therefore use a pump fluence around $270 \mu\text{J}/\text{cm}^2$, indicated by the vertical dotted black line, to remain in the linear regime for all of our measurements. We note that this fluence may seem high to those used to working with samples of randomly oriented TIPS-Pn molecules, but in its crystalline form the $S_0 \rightarrow S_1$ TDM is oriented nearly normal to the substrate, and couples only weakly to the incoming light. These high fluences therefore produce modest exciton densities around 1%. Furthermore, the one-dimensional nature of the exciton diffusion along the π -stacked direction means that an exciton must travel roughly 40 nm before encountering another exciton, which helps to prevent diffusion-based annihilation from occurring during the experimental time frame. Details are in the Supporting Information, Section S1.4.

To better understand the underlying dynamics from the TAM data, we find it helpful to define the *normalized offset*, $\zeta = \frac{C+A/2}{|A|/2}$.⁵⁵ For fixed τ , consider the plot of ΔT vs θ and the functional form that describes it in eq 1. The numerator of ζ is the value of ΔT averaged over θ ; the denominator serves to normalize it by the half amplitude of ΔT 's cosine-squared functional form. This procedure is shown intuitively in Figure 3a. Positive values of ζ mean that GSB is the dominant contribution to ΔT , while negative values indicate that ESA is the dominant contribution. The most important quality of the normalized offset is that it is insensitive to the absolute excited state population (assuming measurement in the linear regime). If all excited populations decay uniformly, then all GSB and ESA signals decay uniformly. Yet, because it is normalized, ζ will be invariant in time over the course of the uniform decay. A shift in ζ can therefore be used to infer a change in the makeup of the excited state population.

As an example, we plot ζ as a function of τ in Figure 3b for four different scans: two degenerate ones, and two using white light filtered at 694 nm (which should closely reproduce the degenerate data). The scans agree within experimental error, indicating that normalized offset is a physically meaningful attribute, independent of changes in laser beam overlap or other experimental conditions. We observe three population shifts in the data. The first two, occurring over approximately 100 fs and 1 ps time scales, correspond to previously measured decays. At longer time delays, ζ is roughly constant until it undergoes a final shift with a 330 ps time scale, whereupon it is stable until at least 2.5 ns. The shift is statistically significant: the difference between the average signals for time points before (40–125 ps) and after (500 ps–2.5 ns) the shift is 3.8 standard deviations. Because long-lived triplets are known to be produced in TIPS-Pn films, we conclude that the excited state population beyond 500 ps delay consists almost exclusively of dissociated triplets. ΔT at long times is therefore due to two TDMs: one associated with GSB on the $S_0 \rightarrow S_1$ transition, indicative of how many triplet excitons exist, and another associated with the ESA from the triplet excitons. We plot ΔT vs θ at $\tau = 1.4$ ns (Figure S4), and fit to the form

$$\Delta T(\theta) = A_{\text{GSB}} \cos^2(\theta - \theta_{\text{GSB}}) + A_{T-\text{ESA}} \cos^2(\theta - \theta_{T-\text{ESA}}) \quad (2)$$

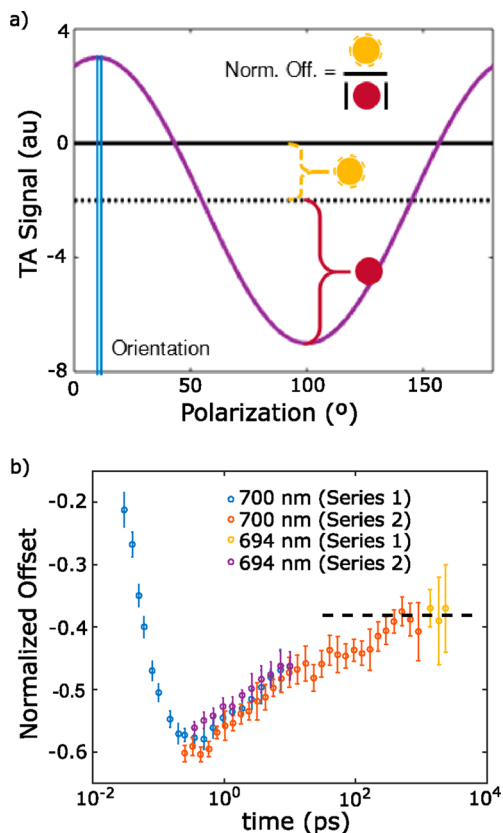


Figure 3. (a) Cartoon describing how normalized offset, ζ , is calculated. Purple curve is $\Delta T(\theta)$ which can be modeled via eq 1. The offset is the average value of the curve (dashed line). It is normalized by the half amplitude of the curve, indicated by the red dot. We also extract the orientation of the crystalline domain in the lab frame (vertical blue double line). (b) Measured normalized offset in TIPS-Pn, for four different data sets, two with a degenerate 700 nm probe, and two with a 694 nm probe. The dashed line is a guide to indicate the plateau of ζ at long times.

where θ_{GSB} is fixed based on linear absorption measurements. We extract the quantities $\theta_{T-\text{ESA}}$ and $A_{T-\text{ESA}}/A_{\text{GSB}}$, both of which provide information about the dissociated triplet absorption and will be crucial to our subsequent analysis.

We next construct a kinetic model that can explain our observations. One challenge is to determine whether singlet fission manifests in the 100 fs or 1 ps process. For reasons explained in the following paragraph, we assign fission to the 1 ps process and use the model shown in Figure 1e: The pump generates a vibrationally excited singlet population, S_1^n , which thermalizes to S_1^0 over the 100 fs time scale. Singlet fission and triplet fusion act to generate an equilibrium between singlets S_1^0 and correlated triplet pairs, $(TT)^1$. This equilibrium grows in on a 1 ps time scale, and either of the two states can decay to the ground state via internal conversion. A triplet pair can separate to form two dissociated triplets, $T+T$. In addition to including in our fitting the two TDMs mentioned in the preceding paragraph, we also allow for ESA from S_1^n , S_1^0 , and $(TT)^1$. A best fit of the model to the data returns unique values for the rate constants, as well as amplitudes and orientations of the unknown TDMs. (For more details see Supporting Information Section S2.)

We now motivate the form of the kinetic model presented schematically in Figure 1e. Note that when the probe polarization is orthogonal to the GSB TDM (in Figure 2a, θ

Table 1. TIPS-Pn Parameters Extracted from a Kinetic Fit of Degenerate Transient Absorption Data at 700 nm^a

domain	τ_{te} (ps)	f	τ_{int} (ps)	τ_{dis} (ps)	η (%)
1	1.4 ± 0.2	0.74 ± 0.03	149 ± 24	330 ± 53	112 ± 14
2	2.0 ± 0.3	0.69 ± 0.04	106 ± 16	360 ± 53	79 ± 13
3	1.6 ± 0.3	0.60 ± 0.04	196 ± 32	240 ± 60	110 ± 17

^aSinglet fission is characterized by a triplet equilibration time scale (τ_{te}) and equilibrium triplet fraction (f). Exciton decay occurs on the time scales of internal conversion (τ_{int}) and triplet dissociation (τ_{dis}). From these we calculate the triplet formation internal quantum efficiency (η). The internal conversion time scale is a composite due to decay of both S_1 and $(TT)^1$.

= 145°), ΔT consists only of ESA, making it easier to interpret the physical meaning of the signal. If near-unity efficiency singlet fission were to occur within the first 100 fs, then the ESA from each singlet would be replaced by that of a triplet pair over this short time scale. Because we measure the relative strength of the triplet ESA via A_{T-ESA}/A_{GSB} , we are able to calculate the effect that fission would have on the total ESA signal. We find the result to be incompatible with the sharp drop in ΔT that we observe during the first 100 fs of dynamics. The attempted fit can be seen in Figure S5, and shows that sub-picosecond fission is incompatible with our data. Furthermore, a population of solely triplets would be static over the first 1 ns if fission were to occur in the first 100 fs, but we observe multiple subsequent changes in the normalized offset after 100 fs (Figure 3b), indicative of further significant excited state population shifts. Therefore, the 100 fs time scale cannot correspond to fission, leaving the 1 ps time scale as the only viable option. One possible explanation for the 100 fs time scale is thermalization (intramolecular vibrational relaxation), which would lead to a loss of stimulated emission, and explain the initial drop in signal for polarizations aligned with the $S_0 \rightarrow S_1$ TDM, such as at $\theta = 55^\circ$ in Figure 2a. The lack of fluorescence observed from TIPS-Pn⁶⁰ indicates that subsequent states, the vibrationally relaxed singlet and correlated triplet pair, lack significant optical coupling to the ground state, and hence do not give rise to further stimulated emission. Ultrafast thermalization would be consistent with time scales measured in similar materials,⁶¹ and could also explain why pumping with higher energy photons has generally resulted in slower time scales for the first process of up to 220 fs.³⁶ For a thorough justification of this choice, see the Supporting Information, Section S3 and Table S1.

We now consider the dynamics over longer time scales, particularly the shift in ζ at 330 ps. This shift indicates the presence of further excited state dynamics after triplets have formed, and therefore precludes the possibility of high-efficiency, unidirectional singlet fission (see Figure S6). In Section S3, Alternative 3, we consider the possibility that traps or other irregularities could lead to nonuniform fission dynamics that could explain the shift in ζ , but we eventually rule out this possibility. The simplest explanation is to allow for triplet fusion, the ability of the $(TT)^1$ species to convert back to the singlet state S_1 . Equilibrium is established between these two states over the first few ps, and the subsequent decrease in signal strength at all polarizations indicates the presence of a decay channel. Because we work in a linear regime with respect to pump power, this decay cannot be diffusion-based recombination. Fluorescence has not been observed in TIPS-Pn,⁶⁰ so we conclude that this decay is nonradiative internal conversion, which could originate from either or both of S_1 and $(TT)^1$. As the correlated triplet pairs dissociate, the population shifts from being a mixture of singlets and triplet pairs to purely dissociated triplets, although the triplets may retain long-range

spin correlations.^{1,44} The normalized offset is specifically sensitive to this shift and the attendant loss of singlet population. Therefore, by examining Figure 3b we see that ζ shifts around 330 ps, and conclude that this time scale corresponds to triplet dissociation. Such slow triplet dissociation indicates that the initially formed correlated triplet pairs must be bound. We note that the dynamics observed in both the normalized offset and TA signal are inconsistent with unidirectional fission on a 100 fs time scale.

In order to make quantitative statements about the ultrafast exciton dynamics in TIPS-Pn, we fit the kinetic model in Figure 1e to the degenerate probe data and plot the results as solid lines in Figure 2a. The extracted parameters are shown in Table 1. We find it most intuitive to define the fission/fusion equilibration time, $\tau_{te} = \frac{1}{k_{sf} + k_{tf}}$, and the $(TT)^1$ generation efficiency, $f = k_{sf}\tau_{te}$. These parameters quantify the time scale for equilibrium to be established between singlets and correlated triplet pairs and the ensuing proportion of triplet pairs, respectively (see Supporting Information Section S2.2 for derivations). We find $\tau_{te} = 1.4$ ps for fission/fusion to come to equilibrium, and that equilibrium favors the correlated triplet pair: $f = 74\%$. The two decay pathways from $(TT)^1$, internal conversion and triplet dissociation, are much slower. We find similar results in the three domains that we studied, in accordance with our prior result that different domains of crystalline TIPS-Pn are nearly identical up to an azimuthal rotation in the lab frame.⁵⁹ (The data presented in the main text corresponds to “Domain 1”, though a comparison to Domains 2 and 3 is included in the Supporting Information). The small differences observed between domains could be due to differing degrees of lattice strain, as explored in previous work on a similar organic semiconductor.⁵⁵ This variability is potentially detrimental to device performance, but could be minimized by exercising better control over the solution processing technique.

Having used the degenerate TAM data to construct a model, we consider the white light TAM data of the form $\Delta T(\tau, \theta, \lambda)$, where λ is the central wavelength of the probe pulse. These additional data enable us to ultimately determine the absorbance spectra of individual excited state species, which provides a window into the electronic structure of the correlated triplet pair. Data are shown in Figure 4b–d for three distinct regions of the spectrum: $\lambda = 520, 550,$ and 730 nm. Because we are interested in fission, we focus on the first 10 ps of dynamics; each trace therefore shows a single decay, though the amplitude of the decay and its polarization dependence vary depending on how the probe couples to each TDM. We observe that triplet formation tends to make ΔT more negative as a function of time at bluer probe wavelengths (such as 520 nm) and more positive in time at redder wavelengths (such as 730 nm). At 550 nm we observe a mixture of both behaviors. Unlike at redder wavelengths (such

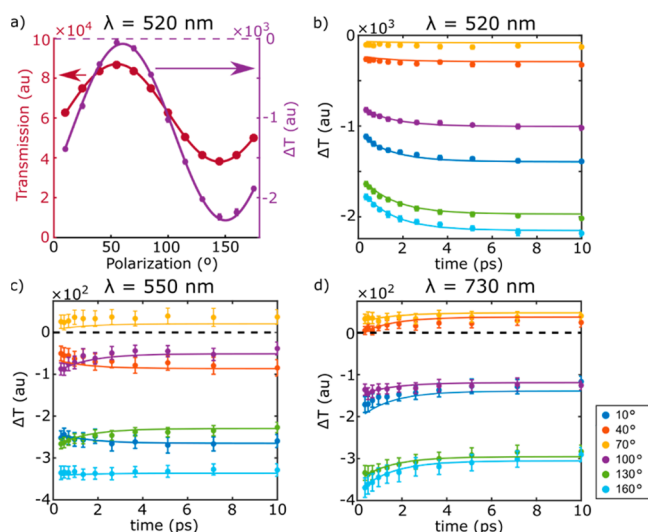


Figure 4. White Light TAM on TIPS-Pn. (a) $\Delta T(\theta)$ (purple) at probe wavelength $\lambda = 520$ nm is compared with the linear transmission (red). Data and kinetic model fits for $\lambda =$ (b) 520 nm, (c) 550 nm, and (d) 730 nm.

as in Figure 2b), in the bluer region of the spectrum ($\lambda \leq 550$ nm) the GSB and ESA TDMs are nearly aligned. This can be seen in Figure 4a, where we plot ΔT vs θ for $\lambda = 520$ nm and compare it to the linear transmission. The highest transmission (weak or possibly no GSB) occurs around $\theta = 55^\circ$, where the TA signal returns to 0 (weak or possibly no ESA). This fact indicates that all of the relevant TDMs in the sample are aligned, and the probe couples to none of them, which is strong corroborating evidence for the uniform crystallinity of the sample. Parallel TDMs, however, make it more challenging to separate the contributions of GSB and ESA, but we develop analytical techniques below to surmount the difficulty.

To fit the data obtained with a white light probe, we first note that the pump pulse is identical for all probe wavelengths (including the degenerate probe wavelength). Therefore, the dynamics represented at each probe wavelength are the same: differences in ΔT are due solely to the fact that the TDMs are probe-wavelength-dependent. As a result, we fix the time constants of the exponential decays using the values obtained in the degenerate data fitting above so that we may determine the strength and orientations of the TDMs at each probe wavelength. Unfortunately, because the GSB and all ESA TDMs are nearly aligned with each other when $\lambda \leq 600$ nm (Figure 4a), our model cannot uniquely fit the data without fixing an additional parameter. Fortunately we can fix the expected value of the GSB signal based on the experimental conditions described below. To do so, we note that the probe absorption scales linearly with the amount of ground state population, such that vacancies created by the pump proportionately decrease the probe absorption to generate the GSB. On the basis of this physics, we are able to derive an expression for the GSB contribution to ΔT that depends on beam characteristics (pump power P , beam diameters σ) and the linear absorption of the probe, $\text{Abs}(\theta, \lambda)$, all of which are measured independently:

$$\Delta T_{\text{GSB}}(\theta, \lambda) = \xi \frac{P \times \text{Abs}(\theta, \lambda)}{\pi(\sigma_{\text{pump}}^2 + \sigma_{\text{probe}}^2)} \quad (3)$$

A derivation of eq 3 can be found in Supporting Information Section S4, and accompanying Figures S7 and S8. The only unknown in this expression is ξ , a measure of how efficiently the pump pulse creates excitons. This exciton creation factor depends on the pump wavelength and the sample thickness and orientation. For a given domain in our sample, we use our fit of the degenerate TA data to calculate the value of ξ (tabulated in Table S2). This is subsequently used to calculate ΔT_{GSB} at all other probe wavelengths.

Using the above procedure to fix ΔT_{GSB} permits us to model the data well at each probe wavelength. The fits are shown as solid lines in Figure 4b–d and Figure S9. We find excellent agreement at all probe wavelengths studied, further substantiating the validity of our model. We also extract the orientation and absorbance (projected onto the sample plane) of the ESA TDMs due to both singlets and bound correlated triplets. We measure the ESA TDM due to dissociated triplets by performing TAM with longer time delays and fitting the kinetic model to that data (Figure S10). As for the GSB TDM, we determine its orientation and absorbance from polarization-resolved absorbance measurements and from eq 3, respectively. In this way, we independently measure the TDM for absorbance from four states: ground state, singlet exciton, bound triplet exciton, and dissociated triplet exciton.

The absorbance and orientation of the TDMs considered here are plotted in Figure 5a,b (results on additional domains can be found in Supporting Information Section S6, Figures S11–13, and Table S3). Considering the absorbance spectra, we note that the excited states share a prominent feature around 525 nm. We also note that the bound and dissociated triplets display similar, but not entirely identical absorption profiles—the difference between the two is magnified in the inset. As for the orientations, the band edge absorption TDM is known to be oriented along the short axis of the pentacene core,⁵⁶ which for the purposes of Figure 5b we define to be 0° . But this appears to be the exception—most TDMs are oriented roughly along the long axis of the pentacene core. Similar TDM orientations are observed in pentacene.⁵⁷

Having established a kinetic model for crystalline TIPS-Pn and measured the relevant rates and TDMs, we next analyze these results to better understand the behavior of the correlated triplet pair.

DISCUSSION

Using polarization-resolved TAM, we have established that singlet fission in TIPS-Pn occurs on a picosecond time scale, which is slower than reported in some previous work.³⁴ We find that the two triplets created by fission remain adjacent for hundreds of picoseconds, indicative of an attractive interaction between them. Using a white light probe, we have measured the absorbance spectra of several species, and teased apart differences between the absorbance of the bound and dissociated triplet excitons. In this section we discuss the kinetics and electronic structure of the correlated triplet pair, how our findings could generalize to other π -stacked systems, and the implications for singlet fission-based photovoltaics.

We first focus on the experimental evidence that supports a hypothesis of an attractive interaction between the triplets in the correlated pair. Our data suggest that the balance of singlet and correlated triplet populations reaches equilibrium in roughly 1.4 ps. The efficiency of the singlet fission process just after this time delay is twice the $(TT)^1$ generation efficiency, $2f \sim 140\%$. This value is in agreement with the

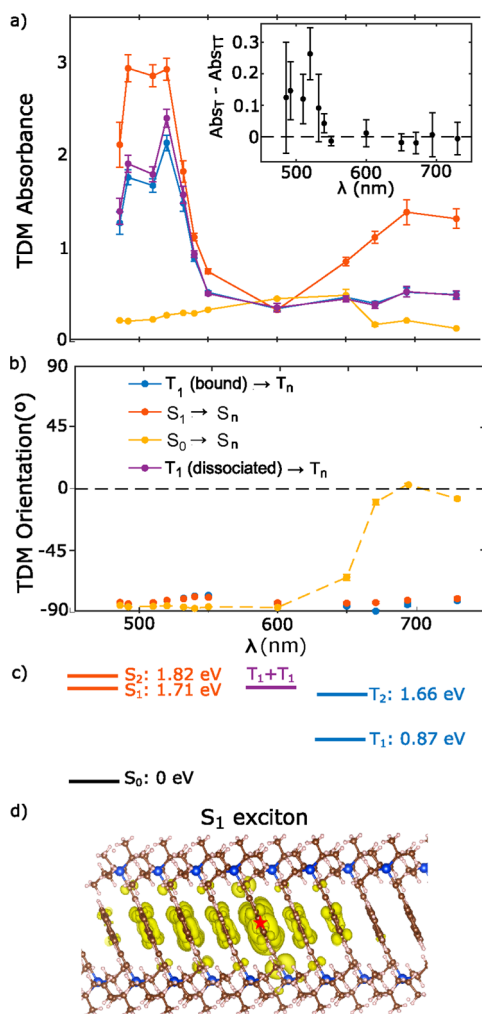


Figure 5. Transition dipole moments of TIPS-Pn. TDM (a) absorbance (for unpolarized light) and (b) orientation for transitions originating from the following states: ground state S_0 (yellow), first excited singlet state S_1 (red), bound triplet (blue) and dissociated triplet (purple). Inset shows the difference between the absorbance of the bound and dissociated triplet. Dashed yellow line in (b) is to guide the eye. Bound and dissociated triplet are assumed to have the same TDM orientation. Orientations are shifted from those in Figure 2a to be relative to the short axis of the pentacene core. (c) Energy levels for low-lying singlet and triplet excitons, showing good agreement with our experimentally measured S_1 energy, and the literature value of T_1 energy.¹⁶ (d) A visualization of the S_1 exciton wave function, $\Psi_{S_1}(r_e, r_h)$, calculated by solving the BSE. We localize the hole at the center of the third benzene ring, as indicated by the red star, and plot an isosurface of $|\Psi_{S_1}(r_e, r_h = \text{fixed})|^2$ on a $4 \times 4 \times 2$ supercell.

results of Ramanan et al.³⁵ For $\tau > 100$ ps, the magnitude of ΔT decays at all probe polarizations (Figure 2a). We conclude that excitons can relax to the ground state with an internal conversion time scale of 150 ps, which is presumably a composite of decay from both S_1 and $(TT)^1$. We also observe the normalized offset, ζ , shifting and then stabilizing between approximately 200 and 500 ps (Figure 3b). We deduce that this shift corresponds to the loss of singlets as correlated triplet pairs separate to form long-lived dissociated triplets, precluding further triplet fusion. The fit returns a dissociation time scale of 330 ps, which would be surprisingly long if there were no appreciable binding energy associated with the correlated triplet pair (we would expect freely diffusing triplets to remain

adjacent to one another for only a few picoseconds). Yet there is precedent for these long time scales—in films of TDPP derivatives dissociated triplets take up to 1.6 ns to form, even when an intermediate state forms rapidly.³⁰

On the basis of the long measured triplet separation time scale, we conclude that we are initially observing the correlated triplet pair, and that interactions between the triplets result in a surprisingly stable bound state. To quantify the binding energy, we perform a simple simulation of the diffusion of a bound triplet pair (for details see Supporting Information Section S7 and Figure S15). We consider each TIPS-Pn molecule to be an individual site, and initialize the simulation with two triplets on adjacent molecules. The isolated triplets hop with their measured diffusion constant,³⁹ but based on the delocalized nature of the triplet exciton wave function (Figure S14), we allow for a variable binding energy depending on whether the triplets are separated by one, two, or more sites. Our simulation proceeds via the Gillespie Algorithm.⁶² We find that a binding energy in the range from 50 to 80 meV can explain our experimental results. Although triplet–triplet binding has generally been neglected, a recent report on several acene films, including amorphous TIPS-Pn, also found evidence of an attractive triplet–triplet interaction, reporting energies of about 30 meV.⁵⁰ The non-negligible binding energy is consistent with prior reports that suggest that the triplets are coupled via an exchange interaction,⁴⁴ and suggests that we must consider the possibility that the singlet-mediated triplet exciton diffusion mechanism advanced by Huang et al. for tetracene⁵⁸ and rubrene³⁹ is also significant in TIPS-Pn. They hypothesize that triplets are able to reform singlets, which effectively boosts the apparent triplet diffusion length because singlet transport is much more rapid than triplet transport. They also investigate TIPS-Pn with TAM,³⁹ but presumably trade off the quantity of distinct time delays measured for exquisite spatial resolution, which could explain why they do not resolve the singlet–triplet equilibration and long bound triplet lifetime that we observe.

We next turn to interpret the excited state absorbance spectra shown in Figure 5a. The $S_0 \rightarrow S_n$ absorbance (yellow) is comparatively weak but spans much of the visible range. The $S_1 \rightarrow S_n$ absorbance is the strongest, with a broad peak centered about 700 nm and a taller, sharper peak around 525 nm. The triplet species both share this 525 nm absorbance feature, as has been observed before in TIPS-Pn TA spectra, both in solid state^{35,63} and solution⁶⁴ (blue-shifted). Those TA spectra, however, include contributions from multiple ESA and also GSB TDMs, which are clearly seen to overlap in Figure 5a. In contrast, here the polarized white light TAM allows us to cleanly measure the absorbance spectra of individual species in quantitative terms, and compare them absolutely. Interestingly, we find that the bound triplets (blue) and dissociated triplets (purple) have nearly identical absorbance spectra, but that interacting triplets show slightly diminished absorbance for $\lambda < 550$ nm, as is highlighted in the inset to Figure 5a.

Although the reduction in absorbance of the triplets upon binding is small and close to the error in our measurement, this result is intriguing, especially in light of the results of Pensack et al., who studied several pentacene derivatives and found discrepancies between the TA spectra of interacting and isolated triplets.⁴⁹ One may not be able to draw unequivocal conclusions in either case, but diminished absorbance due to triplet interactions could also explain their results. Is this phenomenon general?

To investigate this question theoretically, we perform first-principles calculations based on density functional theory and many-body perturbation theory (MBPT) within the GW plus Bethe-Salpeter equation (BSE) approach⁶⁵ to accurately compute singlet and triplet excitons in crystalline TIPS-Pn. Using the BerkeleyGW⁶⁶ software, we use this formalism to obtain singlet and triplet excited state energies and wave functions. Computational details are provided in Section S8.2. The GW-BSE approach has been shown in prior work to yield accurate excitation energies for molecular crystals including TIPS-Pn.⁵⁶ In Figure 5c,d we show calculated excitation energies and an isosurface of the computed lowest-energy singlet exciton wave function in real space, assuming a fixed hole position; notably, and as was previously shown,⁵⁶ the exciton wave function is delocalized over multiple monomers (more so than the triplet in Figure S14).

An analogous first-principles treatment of the correlated triplet pair, at the same level of theory as described in the previous paragraph, requires solving a Dyson-like equation for a 4-particle correlation function, an effort well beyond the scope of this work. We can, however, examine the effect of triplet-triplet interactions on excited-state absorbance by expressing $(TT)^1$ approximately as an admixture of uncorrelated triplet pairs and a singlet, since the sum of two T_1 energies is close to the energy of S_1 (~ 1.70 eV, see Figure 5c). Additionally, as $(TT)^1$ has been observed to fluoresce in some systems,^{48,50,67} an admixture with low-lying singlet excitons is very plausible. Using excitation energies and exciton wave functions from our GW-BSE calculations, we compute the effect of mixing singlet states with the uncorrelated triplet pair on the excited-state absorbance (relative to that of a dissociated triplet). We find that introducing singlet character to the uncorrelated triplet pair generally decreases the absorbance, and that this effect is more significant in strongly π -stacked crystals (see Section S8 and Figures S17–S19 of the SI). Put another way, the correlated triplet pair in our model is predicted to generally absorb less, consistent with the measurements here.

Given the above results, we return to reconsider the effect of π -stacking on singlet fission. Though it is generally assumed that π -stacking will lead to strong interactions, rapid fission, and rapid triplet dissociation,^{36,68–70} our findings suggest that this is not uniformly the case. The slip-stacked structure of TIPS-Pn makes it a model π -stacking system, but fission is slower than in pentacene⁷¹ (which has a herringbone structure), internal conversion is rapid enough to cause significant losses, and correlated triplets dissociate slowly. These findings may be more generally true of strongly π -stacked systems: similar time scales were found for TDPP derivatives,³⁰ and a theoretical study has indicated that strong coupling between neighboring molecules can slow fission.²⁹ Fluorinated pentacene undergoes efficient fission in the herringbone polymorph, but when deposited in the π -stacked brickwork polymorph, increased photoluminescence is observed, implying that some triplet pairs fuse to form singlets.⁷²

We hypothesize that π -stacking might hinder singlet fission because of concomitant increased orbital overlap relative to other packing motifs. Though triplet wave functions in pentacene are primarily confined to a single molecule,⁷³ those in TIPS-Pn are comparatively delocalized, extending about 12 Å in the π -stacking direction.⁷⁴ Hence non-negligible overlap is expected between triplets on neighboring TIPS-Pn molecules. More overlap could increase the coupling between excitons and cause more significant CT mixing, which in turn could increase

the binding of the correlated triplet pair. Strong coupling could also hinder the fission yield by promoting internal conversion: in acene dimers, increased overlap has been shown to speed up $(TT)^1$ relaxation.⁷⁵ The crystal structures commonly found in π -stacked systems could also play a role. It has recently been shown that a direct Coulomb coupling between the singlet and two distinct correlated triplet excitons, arising from the herringbone crystal structure, can drive fast fission in crystalline pentacene.¹² Following ref 12, however, the low-lying triplet pair can only couple via this direct mechanism to dark singlet states due to inversion symmetry in TIPS-Pn, indicating that fast triplet formation via a purely Coulomb process would be significantly hindered. For all of these reasons, we propose that our observations on TIPS-pentacene may be generalizable across multiple π -stacked systems.

We wish to point out that we have by no means considered all possible effects that π -stacking could have on singlet fission because π -stacking can be achieved with a wide variety of lattice vectors and intermolecular configurations. Le et al. recently showed the ability to modulate the fission rate by a full order of magnitude in π -stacked perylene diimide films by tuning intermolecular spacing both experimentally and through Redfield theory.⁷⁶ Crystal engineering with π -stacked molecules therefore represents an area with tremendous potential to establish general physical principles that govern electronic dynamics in molecular crystals.

The greater understanding of the kinetics and energetics of the correlated triplet pair that is emerging could lead to more efficient singlet-fission-based photovoltaics. We stress that the relevant quantity to optimize for photovoltaics is the triplet formation internal quantum efficiency, η : the number of triplets harvested per exciton created. In terms of the variables in our kinetic model listed in Table 1,

$$\eta = \frac{2}{1 + \frac{\tau_{\text{dis}}(1-f)}{\tau_{\text{inf}}}} \quad (4)$$

(Supporting Information Section S2.2). This efficiency depends not only on the fission dynamics, but also on the extent and ease of diffusion and on the interplay between triplet dissociation and other decay pathways. We observe triplet binding that is comparable to $k_B T$ at room temperature, which makes singlet-mediated diffusion viable, and hence could allow more triplet pairs to be extracted before they decay, thus boosting η .

According to the values in Table 1, η in the samples that we have studied is approximately 100%. A real device, however, has a triplet extraction layer, which effectively shortens τ_{dis} and therefore increases η . A device made with a 16 nm layer of TIPS-Pn achieved efficiencies of 160%³² because the triplet pairs could rapidly diffuse to an interface to form charge carriers, out-competing internal conversion. Given the kinetic parameters measured herein, we calculate (see Supporting Information Section S9) that efficiencies of over 150% are plausible in devices with TIPS-Pn layers even 100 nm thick. Hence, π -stacking remains a promising design principle for singlet fission, so long as the strength of the resulting triplet-triplet interaction is tailored to maximize triplet extraction while minimizing nonradiative decay.

CONCLUSION

We have used polarized transient absorption microscopy to probe individual crystalline domains of TIPS-pentacene. The

orientational anisotropy of single crystal TIPS-Pn allows us to selectively probe individual transition dipole moments in an innovative new way by varying the polarization of a white light probe pulse. We have developed novel analytical tools to determine the kinetics of singlet fission, and we have used a white light probe in order to make optical measurements of the correlated triplet pair more directly than has previously been achieved. We find evidence that π -stacking leads to substantial triplet–triplet interactions, which manifest themselves through a quantifiable triplet binding energy and perturbations to the absorption spectrum. This binding extends the lifetime of the correlated triplet pair, which we argue could have a significant role in improving the efficiencies of photovoltaic devices.

Although triplet formation must be rapid enough to outcompete other decay pathways, we have illustrated how understanding the kinetics and diffusion of the correlated triplet pair is just as important for creating singlet fission-based photovoltaic devices. In the future, similarly studying a wider variety of molecules would allow us to establish the extent to which bound triplet pairs and diminished absorbance are general features of π -stacked systems. In addition, more detailed theoretical calculations of triplet interactions could further substantiate our results. We could also further test our kinetic modeling of TIPS-Pn by studying photovoltaic efficiency as a function of fission layer thickness in devices. Rapid uniaxial diffusion is crucial to optimized triplet harvesting, emphasizing the need for more research into postprocessing of solution-deposited films, including solvent-vapor annealing.⁷⁷ Our work highlights the complex interplay between structure and dynamics, and paves the way for employing π -stacking as a design principle in singlet fission photovoltaics, by elucidating the ways in which the ensuing strong interactions impact triplet behavior.

■ ASSOCIATED CONTENT

■ Supporting Information

The Supporting Information is available free of charge on the ACS Publications website at DOI: 10.1021/jacs.7b12662.

Detailed description of the experiment; thorough justification for the kinetic model and derivation of the equations used; experimental data and analysis of additional samples; calculations relating to triplet binding energy, absorption of the correlated triplet pair, and triplet harvesting in a device (PDF)

■ AUTHOR INFORMATION

Corresponding Author

*nsginsberg@berkeley.edu

ORCID

Naomi S. Ginsberg: 0000-0002-5660-3586

Notes

The authors declare no competing financial interest.

■ ACKNOWLEDGMENTS

This work has been supported by a David and Lucile Packard Fellowship for Science and Engineering to N.S.G., by STROBE, A National Science Foundation Science & Technology Center under Grant No. DMR 1548924, and by the Center for Computational Study of Excited-State Phenomena in Energy Materials (C2SEP) at the Lawrence Berkeley National Laboratory, which is funded by the U.S. Department of Energy,

Office of Science, Basic Energy Sciences, Materials Sciences and Engineering Division under Contract No. DE-AC02-05CH11231, as part of the Computational Materials Sciences Program. B.D.F. acknowledges a National Science Foundation Graduate Research Fellowship (DGE 1106400). N.S.G. acknowledges an Alfred P. Sloan Research Fellowship, a David and Lucile Packard Foundation Fellowship for Science and Engineering, and a Camille and Henry Dreyfus Teacher-Scholar Award. The authors thank Ryan Pensack for discussion.

■ REFERENCES

- (1) Scholes, G. D. *J. Phys. Chem. A* **2015**, *119* (51), 12699.
- (2) Smith, M. B.; Michl, J. *Annu. Rev. Phys. Chem.* **2013**, *64*, 361.
- (3) Piland, G. B.; Burdett, J. J.; Dillon, R. J.; Bardeen, C. J. *J. Phys. Chem. Lett.* **2014**, *5*, 2312.
- (4) Ehrler, B.; Wilson, M. W. B.; Rao, A.; Friend, R. H.; Greenham, N. C. *Nano Lett.* **2012**, *12*, 1053.
- (5) Pazos-Outon, L. M.; Lee, J. M.; Kirch, A.; Tabachnyk, M.; Friend, R. H.; Ehrler, B. *arXiv* 1512.07466.
- (6) Yost, S. R.; Lee, J.; Wilson, M. W. B.; Wu, T.; McMahon, D. P.; Parkhurst, R. R.; Thompson, N. J.; Congreve, D. N.; Rao, A.; Johnson, K.; Sfeir, M. Y.; Bawendi, M. G.; Swager, T. M.; Friend, R. H.; Baldo, M. a.; Van Voorhis, T. *Nat. Chem.* **2014**, *6* (6), 492.
- (7) Berkelbach, T. C.; Hybertsen, M. S.; Reichman, D. R. *J. Chem. Phys.* **2014**, *141* (7), 074705.
- (8) Teichen, P. E.; Eaves, J. D. *J. Chem. Phys.* **2015**, *143* (4), 044118.
- (9) Feng, X.; Luzanov, A. V.; Krylov, A. I. *J. Phys. Chem. Lett.* **2013**, *4* (22), 3845.
- (10) Zimmerman, P. M.; Bell, F.; Casanova, D.; Head-Gordon, M. *J. Am. Chem. Soc.* **2011**, *133* (49), 19944.
- (11) Aryanpour, K.; Shukla, A.; Mazumdar, S. *J. Phys. Chem. C* **2015**, *119* (13), 6966.
- (12) Refaely-Abramson, S.; da Jornada, F. H.; Louie, S. G.; Neaton, J. B. *Phys. Rev. Lett.* **2017**, *119*, 267401.
- (13) Busby, E.; Xia, J.; Wu, Q.; Low, J. Z.; Song, R.; Miller, J. R.; Zhu, X.; Campos, L. M.; Sfeir, M. Y. *Nat. Mater.* **2015**, *14* (4), 426.
- (14) Monahan, N.; Zhu, X.-Y. *Annu. Rev. Phys. Chem.* **2015**, *66* (1), 601.
- (15) Margulies, E. A.; Miller, C. E.; Wu, Y.; Ma, L.; Schatz, G. C.; Young, R. M.; Wasielewski, M. R. *Nat. Chem.* **2016**, *8*, 1.
- (16) Bakulin, A. A.; Morgan, S. E.; Kehoe, T. B.; Wilson, M. W. B.; Chin, A. W.; Zigmantas, D.; Egorova, D.; Rao, A. *Nat. Chem.* **2016**, *8* (1), 16.
- (17) Tempelaar, R.; Reichman, D. R. *arXiv* 2017, 1703.01173.
- (18) Arias, D. H.; Ryerson, J. L.; Cook, J. D.; Damrauer, N. H.; Johnson, J. C. *Chem. Sci.* **2016**, *7* (2), 1185.
- (19) Feng, X.; Kolomeisky, A. B.; Krylov, A. I. *J. Phys. Chem. C* **2014**, *118* (34), 19608.
- (20) Dillon, R. J.; Piland, G. B.; Bardeen, C. J. *J. Am. Chem. Soc.* **2013**, *135* (46), 17278.
- (21) Ryerson, J. L.; Schrauben, J. N.; Ferguson, A. J.; Sahoo, S. C.; Naumov, P.; Havlas, Z.; Michl, J.; Nozik, A. J.; Johnson, J. C. *J. Phys. Chem. C* **2014**, *118*, 12121.
- (22) Bhattacharyya, K.; Datta, A. *J. Phys. Chem. C* **2017**, *121*, 1412.
- (23) Roberts, S. T.; McAnally, R. E.; Mastron, J. N.; Webber, D. H.; Whited, M. T.; Brutchev, R. L.; Thompson, M. E.; Bradforth, S. E. *J. Am. Chem. Soc.* **2012**, *134*, 6388.
- (24) Wade, J.; Steiner, F.; Niedzialek, D.; James, D. T.; Jung, Y.; Yun, D.-J.; Bradley, D. D. C.; Nelson, J.; Kim, J.-S. *J. Mater. Chem. C* **2014**, *2* (47), 10110.
- (25) Palilis, L. C.; Lane, P. A.; Kushto, G. P.; Purushothaman, B.; Anthony, J. E.; Kafafi, Z. H. *Org. Electron.* **2008**, *9* (5), 747.
- (26) Anthony, J. E.; Brooks, J. S.; Eaton, D. L.; Matson, J. R.; Parkin, S. R. *Proc. SPIE* **2003**, 5217, 124.
- (27) Arago, J.; Troisi, A. *Adv. Funct. Mater.* **2016**, *26*, 2316.
- (28) Renaud, N.; Sherratt, P. A.; Ratner, M. A. *J. Phys. Chem. Lett.* **2013**, *4* (7), 1065.

- (29) Zang, H.; Ke, Y.; Zhao, Y.; Liang, W. *J. Phys. Chem. C* **2016**, *120* (25), 13351.
- (30) Mauck, C. M.; Hartnett, P. E.; Margulies, E. A.; Ma, L.; Miller, C. E.; Schatz, G. C.; Marks, T. J.; Wasielewski, M. R. *J. Am. Chem. Soc.* **2016**, *138*, 11749.
- (31) Wilson, M. W. B.; Rao, A.; Clark, J.; Kumar, R. S. S.; Brida, D.; Cerullo, G.; Friend, R. H. *J. Am. Chem. Soc.* **2011**, *133*, 11830.
- (32) Yang, L.; Tabachnyk, M.; Bayliss, S. L.; Böhm, M. L.; Broch, K.; Greenham, N. C.; Friend, R. H.; Ehrler, B. *Nano Lett.* **2015**, *15* (1), 354.
- (33) Walker, B. J.; Musser, A. J.; Beljonne, D.; Friend, R. H. *Nat. Chem.* **2013**, *5* (12), 1019.
- (34) Musser, A. J.; Liebel, M.; Schnedermann, C.; Wende, T.; Kehoe, T. B.; Rao, A.; Kukura, P. *Nat. Phys.* **2015**, *11*, 352.
- (35) Ramanan, C.; Smeigh, A. L.; Anthony, J. E.; Marks, T. J.; Wasielewski, M. R. *J. Am. Chem. Soc.* **2012**, *134*, 386.
- (36) Pensack, R. D.; Tilley, A. J.; Parkin, S. R.; Lee, T. S.; Payne, M. M.; Gao, D.; Jahnke, A. A.; Oblinsky, D. G.; Li, P.-F.; Anthony, J. E.; Seferos, D. S.; Scholes, G. D. *J. Am. Chem. Soc.* **2015**, *137* (21), 6790.
- (37) Tayebjee, M. J. Y.; Schwarz, K. N.; MacQueen, R. W.; Dvorak, M.; Lam, A. W. C.; Ghiggino, K. P.; McCamey, D. R.; Schmidt, T. W.; Conibeer, G. J. *J. Phys. Chem. C* **2016**, *120* (1), 157.
- (38) Pensack, R. D.; Grieco, C.; Purdum, G. E.; Mazza, S. M.; Andrew, J.; Ostroumov, E. E.; Seferos, D. S.; Loo, Y.; Asbury, J. B.; John, E. *Mater. Horiz.* **2017**, *4*, 915.
- (39) Zhu, T.; Wan, Y.; Guo, Z.; Johnson, J.; Huang, L. *Adv. Mater.* **2016**, *28*, 7539.
- (40) Chan, W.-L.; Ligges, M.; Jailaubekov, A.; Kaake, L.; Miaja-Avila, L.; Zhu, X.-Y. *Science* **2011**, *334*, 1541.
- (41) Monahan, N. R.; Sun, D.; Tamura, H.; Williams, K. W.; Xu, B.; Zhong, Y.; Kumar, B.; Nuckolls, C.; Harutyunyan, A. R.; Chen, G.; Dai, H.-L.; Beljonne, D.; Rao, Y.; Zhu, X.-Y. *Nat. Chem.* **2017**, *8*, 1.
- (42) Wang, R.; Zhang, C.; Zhang, B.; Liu, Y.; Wang, X.; Xiao, M. *Nat. Commun.* **2015**, *6* (May), 8602.
- (43) Burdett, J. J.; Bardeen, C. J. *J. Am. Chem. Soc.* **2012**, *134* (20), 8597.
- (44) Weiss, L. R. L.; Bayliss, S. L. S.; Kraffert, F.; Thorley, K. J. K.; Anthony, J. E. J. E.; Bittl, R.; Friend, R. H. R. H.; Rao, A.; Greenham, N. C. N. C.; Behrends, J. *Nat. Phys.* **2017**, *1*, 1.
- (45) Tayebjee, M. J. Y.; Sanders, S. N.; Kumarasamy, E.; Campos, L. M.; Sfeir, M. Y.; McCamey, D. R. *Nat. Phys.* **2017**, *1*, 182.
- (46) Wilson, M. W. B.; Rao, A.; Johnson, K.; Gelinias, S.; Di Pietro, R.; Clark, J.; Friend, R. H. *J. Am. Chem. Soc.* **2013**, *135* (44), 16680.
- (47) Stern, H. L.; Musser, A. J.; Gelinias, S.; Parkinson, P.; Herz, L. M.; Bruzek, M. J.; Anthony, J.; Friend, R. H.; Walker, B. J. *Proc. Natl. Acad. Sci. U. S. A.* **2015**, *112* (25), 7656.
- (48) Stern, H. L.; Cheminal, A.; Yost, S. R.; Broch, K.; Bayliss, S. L.; Chen, K.; Tabachnyk, M.; Thorley, K.; Greenham, N.; Hodgkiss, J.; Anthony, J.; Head-Gordon, M.; Musser, A. J.; Rao, A.; Friend, R. H. *arXiv* **2017**, 1704.01695.
- (49) Pensack, R. D.; Ostroumov, E. E.; Tilley, A. J.; Mazza, S.; Grieco, C.; Thorley, K. J.; Asbury, J. B.; Seferos, D. S.; Anthony, J. E.; Scholes, G. D. *J. Phys. Chem. Lett.* **2016**, *7*, 2370.
- (50) Yong, C. K.; Musser, A. J.; Bayliss, S. L.; Lukman, S.; Tamura, H.; Bubnova, O.; Hallani, R. K.; Meneau, A.; Resel, R.; Maruyama, M.; Hotta, S.; Herz, L. M.; Beljonne, D.; Anthony, J. E.; Clark, J.; Siringhaus, H. *Nat. Commun.* **2017**, *8*, 15953.
- (51) Shi, H.; Yan, R.; Bertolazzi, S.; Brivio, J.; Gao, B.; Kis, A.; Jena, D.; Xing, H. G.; Huang, L. *ACS Nano* **2013**, *7* (2), 1072.
- (52) Grumstrup, E. M.; Gabriel, M. M.; Pinion, C. W.; Parker, J. K.; Cahoon, J. F.; Papanikolas, J. M. *Nano Lett.* **2014**, *14*, 6287.
- (53) Guo, Z.; Manser, J. S.; Wan, Y.; Kamat, P. V.; Huang, L. *Nat. Commun.* **2015**, DOI: 10.1038/ncomms8471.
- (54) Grancini, G.; Polli, D.; Fazzi, D.; Cabanillas-gonzalez, J.; Cerullo, G.; Lanzani, G. *J. Phys. Chem. Lett.* **2011**, *2* (9), 1099.
- (55) Wong, C. Y.; Folie, B. D.; Cotts, B. L.; Ginsberg, N. S. *J. Phys. Chem. Lett.* **2015**, *6*, 3155.
- (56) Sharifzadeh, S.; Wong, C. Y.; Wu, H.; Cotts, B. L.; Kronik, L.; Ginsberg, N. S.; Neaton, J. B. *Adv. Funct. Mater.* **2015**, *25* (13), 2038.
- (57) McDonough, T. J.; Zhang, L.; Roy, S. S.; Kearns, N. M.; Arnold, M.; Zanni, M.; Andrew, T. L. *Phys. Chem. Chem. Phys.* **2017**, *19*, 4809.
- (58) Wan, Y.; Guo, Z.; Zhu, T.; Yan, S.; Johnson, J.; Huang, L. *Nat. Chem.* **2015**, *7*, 785.
- (59) Wong, C. Y.; Penwell, S. B.; Cotts, B. L.; Noriega, R.; Wu, H.; Ginsberg, N. S. *J. Phys. Chem. C* **2013**, *117* (42), 22111.
- (60) Platt, A. D.; Day, J.; Subramanian, S.; Anthony, J. E.; Ostroverkhova, O. *J. Phys. Chem. C* **2009**, *113* (31), 14006.
- (61) West, B. A.; Womick, J. M.; McNeil, L. E.; Tan, K. J.; Moran, A. M. *J. Chem. Phys.* **2014**, *140* (11), 10580.
- (62) Gillespie, D. T. *J. Phys. Chem.* **1977**, *81* (25), 2340.
- (63) Herz, J.; Backup, T.; Paulus, F.; Engelhart, J.; Bunz, U. H. F.; Motzkus, M. *J. Phys. Chem. Lett.* **2014**, *5* (14), 2425.
- (64) Walker, B. J.; Musser, A. J.; Beljonne, D.; Friend, R. H. *Nat. Chem.* **2013**, *5* (12), 1019.
- (65) Rohlfling, M.; Louie, S. G. *Phys. Rev. B: Condens. Matter Mater. Phys.* **2000**, *62* (8), 4927.
- (66) Deslippe, J.; Samsonidze, G.; Strubbe, D. A.; Jain, M.; Cohen, M. L.; Louie, S. G. *Comput. Phys. Commun.* **2012**, *183* (6), 1269.
- (67) Tayebjee, M. J. Y.; Clady, R. G. C. R.; Schmidt, T. W. *Phys. Chem. Chem. Phys.* **2013**, *15* (35), 14797.
- (68) Kolata, K.; Breuer, T.; Witte, G.; Chatterjee, S. *ACS Nano* **2014**, *8* (7), 7377.
- (69) Smith, M. B.; Michl, J. *Chem. Rev.* **2010**, *110*, 6891.
- (70) Johnson, J. C.; Nozik, A. J.; Michl, J. *Acc. Chem. Res.* **2013**, *46* (6), 1290.
- (71) Wilson, M. W. B.; Rao, A.; Clark, J.; Kumar, R. S. S.; Brida, D.; Cerullo, G.; Friend, R. H. *J. Am. Chem. Soc.* **2011**, *133*, 11830.
- (72) Rinn, A.; Breuer, T.; Wiegand, J.; Beck, M.; Hübner, J.; Oestreich, M. *arXiv* **2016**, 1612.03478.
- (73) Sharifzadeh, S.; Darancet, P.; Kronik, L.; Neaton, J. B. *J. Phys. Chem. Lett.* **2013**, *4* (13), 2197.
- (74) Bayliss, S. L.; Thorley, K. J.; Anthony, J. E.; Bouchiat, H.; Greenham, N. C.; Chepelienskii, A. D. *Phys. Rev. B: Condens. Matter Mater. Phys.* **2015**, *92* (11), 1.
- (75) Korovina, N. V.; Das, S.; Nett, Z.; Feng, X.; Joy, J.; Haiges, R.; Krylov, A. I.; Bradforth, S. E.; Thompson, M. E. *J. Am. Chem. Soc.* **2016**, *138* (2), 617.
- (76) Le, A. K.; Bender, J. A.; Arias, D. H.; Cotton, D. E.; Johnson, J. C.; Roberts, S. T. *J. Am. Chem. Soc.* **2018**, *140* (2), 814.
- (77) Grieco, C.; Doucette, G. S.; Pensack, R. D.; Payne, M. M.; Rimshaw, A.; Scholes, G. D.; Anthony, J. E.; Asbury, J. B. *J. Am. Chem. Soc.* **2016**, *138*, 16069.